Forschungszentrum Karlsruhe
in der Helmholtz-Gemeinschaft

Wissenschaftliche Berichte
FZKA 7450

Defect Assessment Procedures for High Temperature Applications

Final Report
TW5-TTMS-005, D5

F. Siska, J. Aktaa

Institut für Materialforschung
Programm Kernfusion
Association Forschungszentrum Kalrsruhe / EURATOM

Juni 2009

Forschungszentrum Karlsruhe
in der Helmholtz-Gemeinschaft
Wissenschaftliche Berichte
FZKA 7450

Defect assessment procedures for high temperature applications

Final report
TW5-TTMS-005, D5

Filip SISKA, Jarir AKTAA

Association Forschungszentrum Karlsruhe/EUROATOM
Programm Kernfusion
Institut für Materialforschung

Forschungszentrum Karlsruhe GmbH, Karlsruhe
2009

Forschungszentrum Karlsruhe GmbH
Postfach 3640, 76021 Karlsruhe

Mitglied der Hermann von Helmholtz-Gemeinschaft
Deutscher Forschungszentren (HGF)

ISSN 0947-8620

urn:nbn:de:0005-074501

Report for TASK of the EFDA Technology Programme

Reference:	Field: Tritium Breeding and Materials Area: Materials Development Task: TW5–TTMS–005 Task Title: Rules for Design Fabrication and Inspection Subtask Title: High temperature fracture mechanical (creep–fatigue) rules: Formulation and implementation Deliverable No.: D5		
Document:	Defect assessment procedures for high temperature applications		
Level of confidentality	Free distribution ☒ Confidental ☐ Restricted distribution ☐		
Author(s):	F.Siska, J.Aktaa		
Date:	18.12.2008		
Distribution list:	Rainer Laesser (Field Co–ordinator) Eberhard Diegele (Responsible Officer) Bob van der Schaaf (Project Leader) Farhad Tavassoli (Task Co–ordinator)		
Abstract:	The objective of this task is to develop the high temperature part of a design code for fusion reactor components build from EUROFER. This development includes fracture mechanical rules for the assessment of detected defects under creep and creep–fatigue conditions. The assessment procedures R5, R6, JNC, A16, Partial Safety Factors were investigated and tested. As the most suitable procedure is chosen R5 and it is further verified by comparison with finite element simulations using the EUROFER material data. These simulations consist of evaluation of $C(t)$ parameter for several geometries (CT specimen,cylinder with fully circumferential crack subjected to the internal pressure, cylinder with semi–elliptical circumferential crack subjected to the internal pressure and Mock-Up test blanket module (TBM) geometry). The R5 procedure provides very good accordance with FE simulations and it is suitable for lifetime assessment. Therefore the guide for R5 application is implemented in the report.		
Revision No:-	–		
	Written by:	Revised by:	Approved by:
	Filip Siska	Jarir Aktaa	Oliver Kraft

Abstract

The objective of this task is to develop the high temperature part of a design code for fusion reactor components build from EUROFER. This development includes fracture mechanical rules for the assessment of detected defects under creep and creep–fatigue conditions. The assessment procedures R5, R6, JNC, A16, Partial Safety Factors were investigated and tested. As the most suitable procedure is chosen R5 and it is further verified by comparison with finite element simulations using the EUROFER material data. These simulations consist of evaluation of C(t) parameter for several geometries (CT specimen,cylinder with fully circumferential crack subjected to the internal pressure, cylinder with semi– elliptical circumferential crack subjected to the internal pressure and Mock-Up test blanket module (TBM) geometry). The R5 procedure provides very good accordance with FE simulations and it is suitable for lifetime assessment. Therefore the guide for R5 application is implemented in the report.

Zusammenfassung

Fehlerbeurteilungsprozedur für Hochtemperaturanwendungen

Das Ziel dieser Arbeit ist ein Hochtemperaturbestandteil eines Design–Codes für die Fusionsreaktorkomponenten aus EUROFER zu entwickeln. Diese Entwicklung umfasst bruchmechanische Regeln für die Bewertung der festgestellten Fehler unter Kriech– und Kriechermüdungs-Bedingungen. Die Bewertungsverfahren sind R5, R6, JNC, A16, Partial Safety Factors, welche untersucht und getestet werden. Als am besten geeignetes Verfahren wird R5 gewählt, das weiterhin durch den Vergleich mit den Finite–Elemente–Simulationen unter Verwendung von den EUROFER-Materialdaten verifiziert wird. Mit diesen Simulationen werden C(t)–Parameter für verschiedene Geometrien (CT–Probe; Zylinder, der mit einem vollständig umlaufenden Innenriss versehen und mit internem Druck beaufschlagt wird; Zylinder, der mit einem halbelliptischen Innenriss in Umfangsrichtung versehen und mit innerem Druck beaufschlagt wird und Mock-Up für die Test–Blanket–Modul

(TBM) Geometrie) berechnet. Das R5-Verfahren liefert ein gutes Ergebnis, das mit der FE-Simulationen sehr gut übereinstimmt und für die Lebensdauerabschätzung gut geeignet ist. Aus diesem Grund ist eine Anleitung zur Anwendung dieses R5-Verfahrens in dem Bericht implementiert.

Contents

Chapter 1

Introduction

All structures like constructions, vehicles, or power plant components contain defects. These are presented due to the technological process of manufacturing or appear during the lifetime of the structure. These flaws may or may not evolve during the lifetime and possibly can cause failure of the whole system. Therefore it is crucial to estimate and predict the evolution of these defects. These estimations can help from several points of view. The lifetime of given system can be estimated and consequently the inspection intervals can be set. From the opposite site these procedures can be used during the design phase to meet the requested lifetime or reliability of the structure. The defect assessment methods are developing since 1960s [1]. Recently with the increased computational effort the full scale FE simulations of structures can be performed which allows estimating the lifetime with better precision. On the other hand, these simulations are very expensive and times consuming therefore the assessment procedures are still very useful and they are continuously developed. The FE simulations together with experiments are nowadays used for evaluation and testing of the assessment methods. The first procedures were developed for the low temperature applications where creep does not play a role. Over the years these methods were extended also for the high temperature applications like in nuclear power industry or recently thermonuclear power structures. Several methods were developed and can be divided into two main groups. The first group methods use failure assessment diagram and provide only the decision whether or not the defect increment reach given value. These

methods are R6 and BS7910-Partial safety factors. The second group methods are able to predict the creep crack growth with time. This group consists of R5, A16 and JNC procedures. This report is organized in the following way. In the next chapter the assessment procedures recently used for high temperature applications are described. The third chapter contains examples of the application of these procedures and their mutual comparison. The fourth chapter consist of comparison of the $C(t)$ values estimates provided by R5 and finite element simulations for several basic structures. Final chapter gives the insight to the future tasks and possible ways of further investigation.

Chapter 2

Assessment procedures

2.1 R5 procedure

The R5 procedure is one of the well established high temperature defect assessment procedure. It is now mostly used in the UK power generation industry. This R5 procedure was also incorporated into the British Standards Document and ASTM [2; 3; 4; 5].

This procedure is based on the reference stress approach. The reference stress is related to the applied load by the relation:

$$\sigma_{ref} = \sigma_y P / P_L(\sigma_y, a) \tag{2.1}$$

where P is applied load and P_L is plastic collapse load for yield stress σ_y and defect size a. Application of this procedure is based on the comparison whether or not the investigated structure can sustain loading conditions for deserved lifetime (t_s) without failure. Four different times have to be evaluated within this method. The schematic illustration of these times is shown in figure 2.1.

First is the time for the propagation of the creep damage through whole structure and failure.

$$t_{CD} = t_r[\sigma_{ref}(a_0)] \tag{2.2}$$

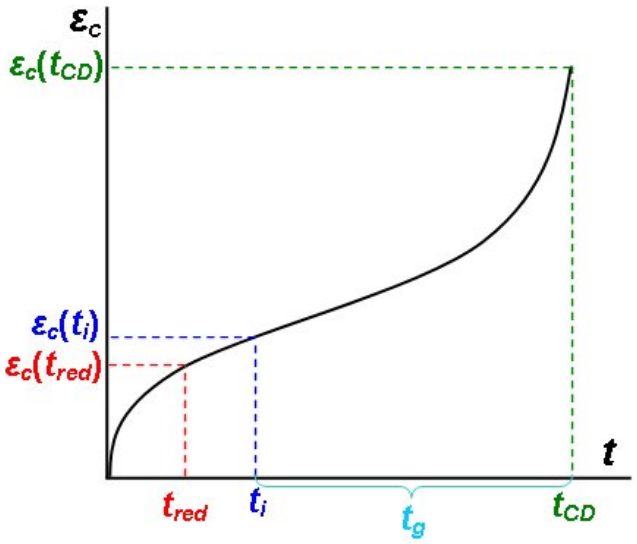

Figure 2.1: Schematic illustration of the times variables used in R5 procedure.

where t_r is the rupture time from conventional stress/time to rupture data and reference stress is calculated for initial crack size a_0. If this time is shorter then requested lifetime t_s the structure is not able to maintain chosen loading conditions and must be redesigned.

The second time is related to the redistribution of the stresses due to the creep. The widespread creep conditions are set after this redistribution. This time can be expressed as:

$$\varepsilon_c[\sigma_{ref}(a_0, t_{red})] = \sigma_{ref}(a_0)/E \tag{2.3}$$

where ε_c is the accumulated creep strain at the reference stress for time t_{red} from uniaxial creep data.

The third time is the initiation time which describes the significant initial crack blunts without any significant crack extension. Usually in the engineering application this corresponds to 0.2 mm crack extension. For the steady state creep conditions, the initiation time can be correlated with the experimental estimates of the crack tip parameter C^* by the equation:

$$t_i C^{*q} = B \tag{2.4}$$

where B and q are constants. The process of the acquisition of this relation from experimental data is shown in figure 2.2.

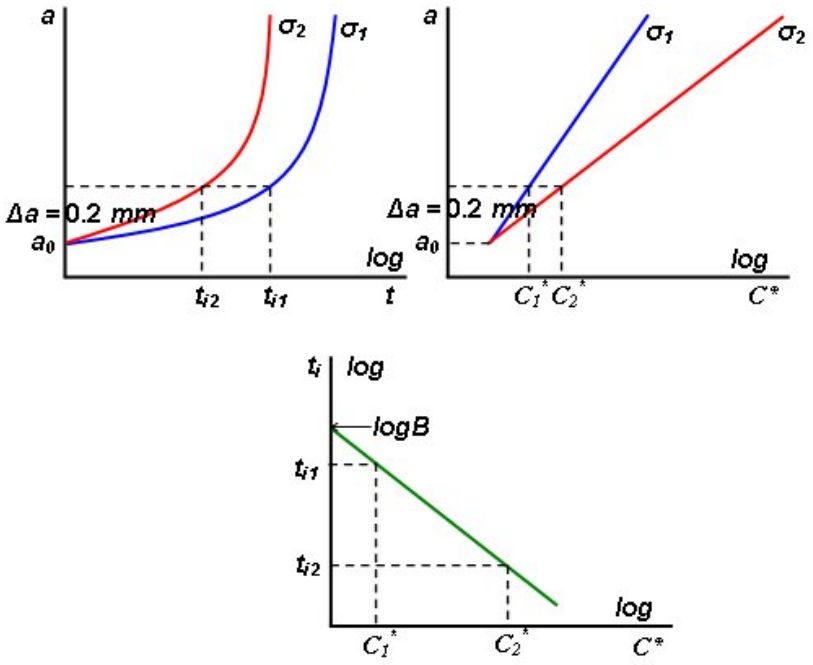

Figure 2.2: Process of obtaining $C^* - t_i$ relation from experimental creep crack growth data.

More general definition of the initiation time is related to the critical crack opening displacement δ_i through the relation:

$$\varepsilon_c[\sigma_{ref}, t_i] = [\delta_i / R(a_0)]^{n/(n+1)} - \sigma_{ref}(a_0)/E \tag{2.5}$$

where the R is characteristic length defined by:

$$R = (K/\sigma_{ref})^2 \tag{2.6}$$

Where K is the stress intensity factor which can be evaluated using the handbook formulas for given geometries or using finite element simulations in other cases. The crack tip parameter is calculated with reference stress technique as:

$$C^* = \sigma_{ref}\dot{\varepsilon}^c_{ref}R \tag{2.7}$$

where $\dot{\varepsilon}^c_{ref}$ is creep strain rate from the uniaxial data at the reference stress. This definition of the crack tip parameter is valid after exceeding the redistribution time. Before the widespread creep conditions the crack tip stress and strain fields are characterized by the parameter $C(t)$. The evolution of this parameter, therefore the transition from the initial elastic state to fully creep state can be described by the equation:

$$\frac{C(t)}{C^*} = \frac{(1 + t/t_{red})^{n+1}}{(1 + t/t_{red})^{n+1} - 1} \tag{2.8}$$

This expression is valid only for materials obeying a Norton secondary creep law in the form:

$$\dot{\varepsilon}^c = D\sigma^n. \tag{2.9}$$

More generalized case can be described by equation:

$$\frac{C(t)}{C^*} = \frac{(1 + \varepsilon^c_{ref}/\varepsilon^e_{ref})^{1/(1-q)}}{(1 + \varepsilon^c_{ref}/\varepsilon^e_{ref})^{1/(1-q)} - 1} \tag{2.10}$$

where ε^c_{ref} is the accumulated creep strain at the reference stress after time t, ε^e_{ref} is the elastic strain at the reference stress and $q \approx n/(n+1)$ is the exponent in the creep crack growth law. The fourth required time (t_g) is time for crack propagation by length Δa. This crack increment under established creep conditions can be computed by the relation:

$$\dot{a} = A(C^*)^q \tag{2.11}$$

where A and q are constants and C^* is estimated according to equation (2.7). Before the stress redistribution ($t < t_{red}$) the crack increment is computed by the generalized equation.

$$\dot{a} = A(C(t))^q \tag{2.12}$$

Computation procedure can be simplified for the case ($t_i + t_g > t_{red}$). The computation is divided into two parts:

$$\dot{a} = 2AC^{*q} \quad t_i \leq t < t_{red} \tag{2.13}$$

$$\dot{a} = AC^{*q} \quad t \geq t_{red} \tag{2.14}$$

If the total time does not exceed t_{red} then it is necessary to use parameter $C(t)$ for estimation of the crack growth.

2.2 A16 procedure

This procedure was developed in France as a result of collaboration of CEA and EdF [6; 7; 8]. This assessment method is used for the predictions of:

- fatigue or creep-fatigue crack initiation
- fatigue crack growth
- creep–fatigue crack growth

2.2.1 Crack initiation-sigma-d method

The crack initiation is based on the so called sigma–d (σ_d) method. The method consists of determination of the stress and strain state in the characteristic distance d from the crack tip and comparison of this state with common material fatigue and creep data. This distance d is a material parameter. For pure fatigue the number of cycles to initiation is estimated from S-N curves for given value of stress at the distance d. This number of cycles is divided by factor 1.5. The parameter crack incubation usage factor A can be computed as ratio of given number of cycles and estimated number of cycles from S-N curves. The creep initiation time T is estimated from creep rupture data for corresponding stress σ_d at distance d. Also the incubation usage factor W can be established for creep as ration between given time and estimated initiation time from creep data. With these two factors the A-W diagram can be drawn (see figure 2.3). If the points with coordinates (A,W) lies inside the envelope, the defect does not initiate over the investigated period.

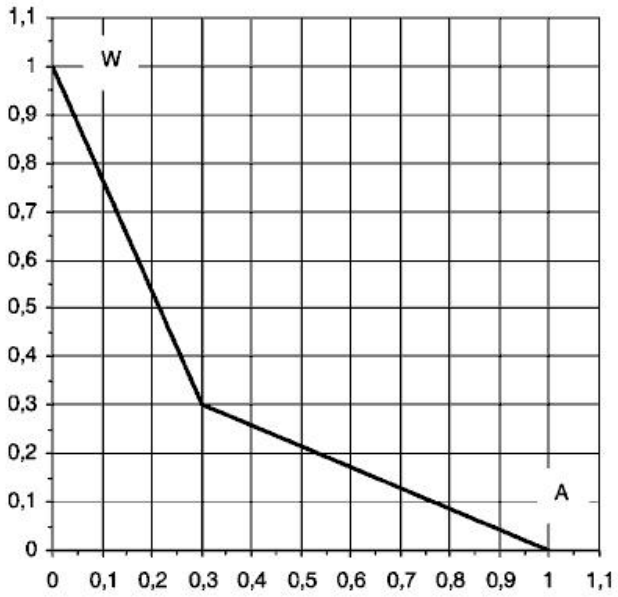

Figure 2.3: A–W diagram for the estimation of the defect imitation during the investigated period (316L stainless steel) [6].

2.2.2 Fatigue crack growth

The fatigue crack growth is computed according to the Paris law. The equation states:

$$\Delta a_f = \sum_{N=0}^{n} C \Delta K_{eff}^k \tag{2.15}$$

where C and k are Paris law parameters, n is given number of cycles and ΔK_{eff} is effective value of stress intensity factor which is computed as:

$$\Delta K_{eff} = q\sqrt{E^* \Delta J} \tag{2.16}$$

where E^* is the modified Young's modulus equal E for plane stress and $E/(1-\nu^2)$ for plain strain, q is the closure ($R < 0$) or mean stress ($R > 0$) coefficient with R being minimum to maximum load ratio. This parameter depends on the material. Finally ΔJ is

computed for the reference stress (σ_{ref} see chapter 2.1). Plastic zone corrections can be also taken into account like in the equation:

$$J = \frac{K_I^2}{E^*}\left(\frac{E\varepsilon_{ref}}{\sigma_{ref}} + \phi\right) \tag{2.17}$$

where σ_{ref},ε_{ref} are reference stress and corresponding reference strain and ϕ is plastic zone correction factor.

2.2.3 Creep crack growth

Creep crack growth is based on the estimation of the C^* parameter according to the relation:

$$C^* = \frac{K_I^2}{E^*}\left(\frac{E\dot{\varepsilon}_{ref}}{\sigma_{ref}}\right) \tag{2.18}$$

where $\dot{\varepsilon}_{ref}$ is strain rate associated to σ_{ref}. The crack increment during the time interval Δt is then calculated from the expression:

$$\Delta a_c = \int_t^{t+\Delta t} A(C^*(t))^q dt \tag{2.19}$$

where A and q are parameters of creep crack growth law. The crack propagation under fatigue and creep is then given as the sum of increments estimated by the fatigue crack growth and creep crack growth.

2.3 JNC procedure

This procedure was developed in Japan [7; 8]. It is very similar to the previous methods but it does not operate with the C^* but with equivalent creep J integral range ΔJ_c. The time dependent creep J integral is computed from elastic J integral (J_{el}) using creep correction parameter f_c.

$$J_c(t) = f_c J_{el} = \frac{E\dot{\varepsilon}_{cref}(t)}{\sigma_{cref}}\frac{K_{max}^2}{E^*} \tag{2.20}$$

where $\dot{\varepsilon}_{cref}(t)$ is reference creep strain rate estimated from creep curve for corresponding temperature and stress relaxation. Reference stress σ_{cref} is taken at the beginning of the

hold time. K_{max} is the stress intensity factor corresponding to the maximum load in the cycle and E^* is modified Young's modulus according to plane stress or strain state. The equivalent creep J integral range ΔJ_c is defined as:

$$\Delta J_c = \int_0^{t_c} J_c(t)dt = \frac{EK_{max}^2}{E^*\sigma_{cref}} \int_0^{t_c} \dot{\varepsilon}_c(t)dt \tag{2.21}$$

where t_c is the hold time interval. The creep crack growth rate can be calculated with the same equation as it is used for C^* parameter:

$$\dot{a} = A\Delta J_c^q \tag{2.22}$$

The JNC method also determines the reference stress after stress relaxation using the net section shape function F_{net} as:

$$\sigma_{ref} = F_{net}(p_m\sigma_m + p_b\sigma_b) \tag{2.23}$$

where σ_m and σ_b are the membrane and bending stresses respectively. The shape function F_{net} depends on the structure and crack shape as well as the parameters p_m and p_b. The reference stress at the beginning of the hold time (σ_{cref}) depends on the yielding conditions:

- small scale yielding conditions $\sigma_{ref} < \sigma_y$

$$\sigma_{cref} = \sigma_{ref}(\sigma_y/\sigma_{ref})^p \tag{2.24}$$

- large scale yielding conditions $\sigma_{ref} >= \sigma_y$

$$\sigma_{cref} = \sigma_{ref} \tag{2.25}$$

where σ_y is yield stress and p is a function of the crack size:

$$p = p_1 + p_2\left(\frac{a}{t}\right) \tag{2.26}$$

with p_1 and p_2 being shape dependent parameters a crack length and t thickness of the structure. Stress relaxation is computed by the relation:

$$d\sigma = \frac{E}{q_C} d\varepsilon_{cref} \tag{2.27}$$

where $d\varepsilon_{cref}$ is creep strain increment calculated by time integration from the creep strain rate $d\dot{\varepsilon}_{cref}$. Parameter q_C is the creep parameter which is equal to 3 for stress or load controlled conditions, 1 for displacement controlled conditions and in between for generalized conditions.

2.4 R6 procedure

This procedure was originally developed for the failure assessment for low temperature applications [9; 10; 11]. Nowadays it was also extended for the high temperature cases [12]. The method can be used in the conditions of the dominant creep crack growth and for small defect increments compare to the original defect size. The R6 method is based on the establishing of failure assessment diagram (FAD) which combines the fracture and plastic mode of failure. This diagram generally gives the prediction whether or not the structure with defined defect will sustain given load. In contrast for the creep cases this method seeks to demonstrate if the small crack extension Δa will occur during the required service life. The service life and crack extension is defined by the user. The failure assessment diagram is then defined by the quantities K_r and L_r which describes fracture and plastic failure mode respectively. These parameters are defined as:

$$K_r = \left(\frac{E\varepsilon_{ref}}{L_r \sigma^c_{0.2}} + \frac{L_r^3 \sigma^c_{0.2}}{2E\varepsilon_{ref}} \right)^{-1/2} \qquad L_r \leq L_r^{max} \tag{2.28}$$

$$K_r = 0 \quad L_r > L_r^{max} \tag{2.29}$$

$$L_r^{max} = \sigma_r / \sigma^c_{0.2} \tag{2.30}$$

where E is Young's modulus, ε_{ref} is the total strain from the stress-strain curve for given temperature and time and for given value of the reference stress. The variable σ_r is the creep rupture stress obtained from the creep rupture data. Reference stress is obtained from equation:

$$\sigma_{ref} = L_r \sigma^c_{0.2} \tag{2.31}$$

where $\sigma^c_{0.2}$ is the 0.2% yield stress from the stress–strain curve for given temperature and time. The example of the failure assessment diagram is shown in the figure 2.4.

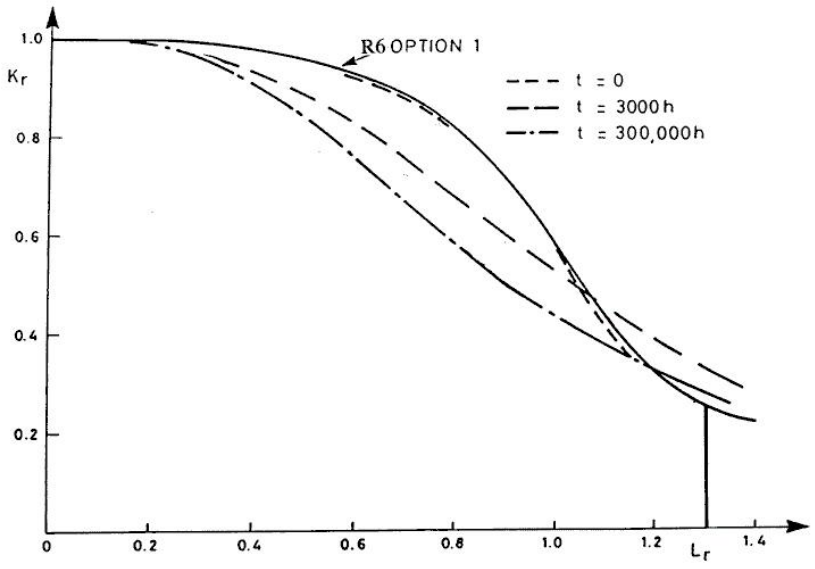

Figure 2.4: FAD diagram in R6 method used for high temperature applications [12].

The structure itself subjected by given conditions is then in the FAD represented by the point with coordinates (L_r, K_r). If this point lies within the diagram the structure will not fail in the classical interpretation or in the creep case the defect extension will not exceed Δa during given time. The parameter L_r is defined as a ratio between the applied loading conditions (F) and those that cause the plastic collapse of cracked component (F_y).

$$L_r = F/F_y(\sigma^c_{0.2}, a_0) \tag{2.32}$$

Parameter K_r describes the fracture mode and its definition states:

$$K_r = K^p(a_0)/K_{mat} \tag{2.33}$$

where $K^p(a_0)$ is the stress intensity factor for given initial defect geometry and applied load and K_{mat} is the creep or fracture toughness. This definition can be generalized taken into account also thermal or residual stresses [5]. Creep toughness can be obtained from experiments. For constant load creep crack growth the creep toughness can be computed as:

$$K^c_{mat} = \left(K^2 + \frac{n}{n+1} \frac{EF\Delta_c}{B(w-a)} \nu \right)^{1/2} \tag{2.34}$$

where ν is the shape function used in determination of C^* from the test data, n is the exponent in creep law, B is the specimen thickness, w is its width, K is the stress intensity factor for specimen and Δ_c is the experimental load line displacement due to the creep for which the crack extension is Δa. This creep toughness also changes during the time and this evolution can be described by the relation:

$$K^c_{mat} \propto t^{-(1/q-1)/2} \tag{2.35}$$

where q is taken from the creep crack growth law using parameter C^*. The value of creep toughness cannot excess for the short times the material fracture toughness. This condition satisfies the consistency with classical R6 procedure. If the fatigue crack growth is presented than K_{mat} is computed according to equation:

$$K_{mat} = K^c_{mat} \left(\frac{\Delta a - \Delta a_f}{\Delta a} \right)^{1/2q} \tag{2.36}$$

where Δa_f is crack increment caused by the fatigue.

2.5 BS7910: partial safety factors

This is the assessment procedure incorporated in British Standards (BS) and recently replaces older version BS6493 [1; 11; 13; 14; 15]. This method is based on the so called partial safety factors which are used in the corrections of loading and structural parameters to estimate if the structure is able to sustain given conditions. The basic decision in this method is to set up the required target reliability of the structure. This chosen required target reliability depends mostly on the consequences of the failure. The reliability increases with increasing failure consequences. These values are shown in the table 2.1 for comparison

Partial safety factors are derived from the reliability analysis using limit state equation of the form:

$$(K_r - \rho)K_{mat} - K_I = 0 \tag{2.37}$$

Failure consequences	Redundant components	Non–redundant components
Moderate	2.3×10^{-1}	10^{-3}
Severe	10^{-3}	7×10^{-5}
Very severe	7×10^{-5}	10^{-5}

Table 2.1: Target reliabilities in BS7910 expressed in terms of events per year or annual failure probabilities.

where K_r is the permitted fracture ratio which is function of the ratio between applied load and plastic collapse load, ρ is the plasticity interaction ratio, K_{mat} is the fracture toughness and K_I is the applied stress intensity factor. The partial safety factors are derived for applied stress, defect size and fracture toughness. The corresponding relations are:

$$\gamma_\sigma = \frac{\sigma^*}{\sigma'}, \quad \gamma_a = \frac{a^*}{a'}, \quad \gamma_K = \frac{K_{mat'}}{K_{mat^*}} \tag{2.38}$$

where $(*)$–signed variables are so called design ones. Those will be used in the design computations. The second group – $(')$–signed variables are characteristic ones which are specified for given structure and loading conditions. Resulting failure equation with safety factors is then given as:

$$(K_r - \rho)\frac{K_{mat}}{\gamma_K} - (\gamma_\sigma Y \sigma)\sqrt{\pi \gamma_a a} = 0 \tag{2.39}$$

where Y is the non–dimensional coefficient to take into account of the crack geometry. The characteristic values ($(')$–signed) are taken assuming the statistical distributions of given variables. The mean values of the corresponding distributions are taken for applied stress and defect size while mean minus one standard deviation is taken for fracture toughness. The statistical distributions for applied load and defect size are supposed to be normal while the fracture toughness is supposed to have Weibull distribution. The coefficient of variation of the applied load (COV_σ) values is also important in the determination of the safety factors. Examples of such safety factors are shown in the table 2.2:

COV_σ	γ_{sigma}	γ_K	γ_a
0.1	1.2	2.3	1.5
0.2	1.25	2.3	1.5
0.3	1.4	2.3	1.5

Table 2.2: Partial safety factors in BS7910 for target failure probability 10^{-3} for the case of a shallow defect ($a < 5$mm).

For the determination whether or not the structure will fail, the failure assessment diagram (FAD) is used as was described in the previous section. If the point (L_r, K_r) corresponding to structure lies within the diagram, the structure will not fail with given target probability.

Chapter 3

Example of application

As an application example the creep crack growth in the CT specimen subjected to constant load. The specimen and loading is shown in the figure 3.1. The dimensions and material parameters are shown in the table 3.1. Only the example of procedure application is shown in this chapter so some material data are chosen artificially.

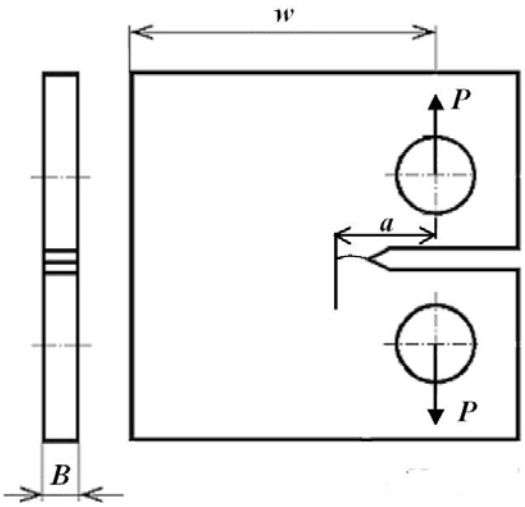

Figure 3.1: CT specimen with defined dimensions and loading.

The stress intensity factor is used in all procedures and for CT specimen is calculated

Specimen dimensions [mm]			
width w	thickness B	initial length a_0	final length a_L
50	25	25	30
Mechanical properties and loading			
Young's modulus E [GPa]	Poisson's ratio ν	Yield stress Y [MPa]	Loading P [kN]
164	0.3	170	3.5
Creep properties			
D	n	A	q
$4.5\times\ 10^{-20}$	10	0.025	0.9

Table 3.1: Parameters for example calculations (specimen dimensions, mechanical and creep properties).

as [16]:

$$K = \frac{P}{B\sqrt{w}} f(a/w) \tag{3.1}$$

$$f(a/w) = \frac{2 + a/w}{(1 - a/w)^{3/2}} [0.886 + 4.64(a/w) - 13.32(a/w)^2 + 14.72(a/w)^3 - 5.6(a/w)^4] \tag{3.2}$$

The reference stress σ_{ref} is also presented in all procedures. It can be determined for CT specimen and plane strain conditions by the relation [16]:

$$\sigma_{ref} = P/[1.455\xi(w - a)] \tag{3.3}$$

$$\xi = \left(\frac{4a^2}{(w-a)^2} + \frac{4a}{(w-a)} + 2 \right)^{1/2} - \left(\frac{2a}{(w-a)} + 1) \right) \tag{3.4}$$

The implementation of the procedures is shown in their flowcharts which are shown in the figure 3.2–3.4.

These flowcharts show the implementation where the initial (a_0) and final (a_L) size of the crack is prescribed by the user. The results is then total time in which the crack growths from the initial to the final size. The other parameters and variables are computed according to the equations given in the previous chapters. The crucial for the lifetime

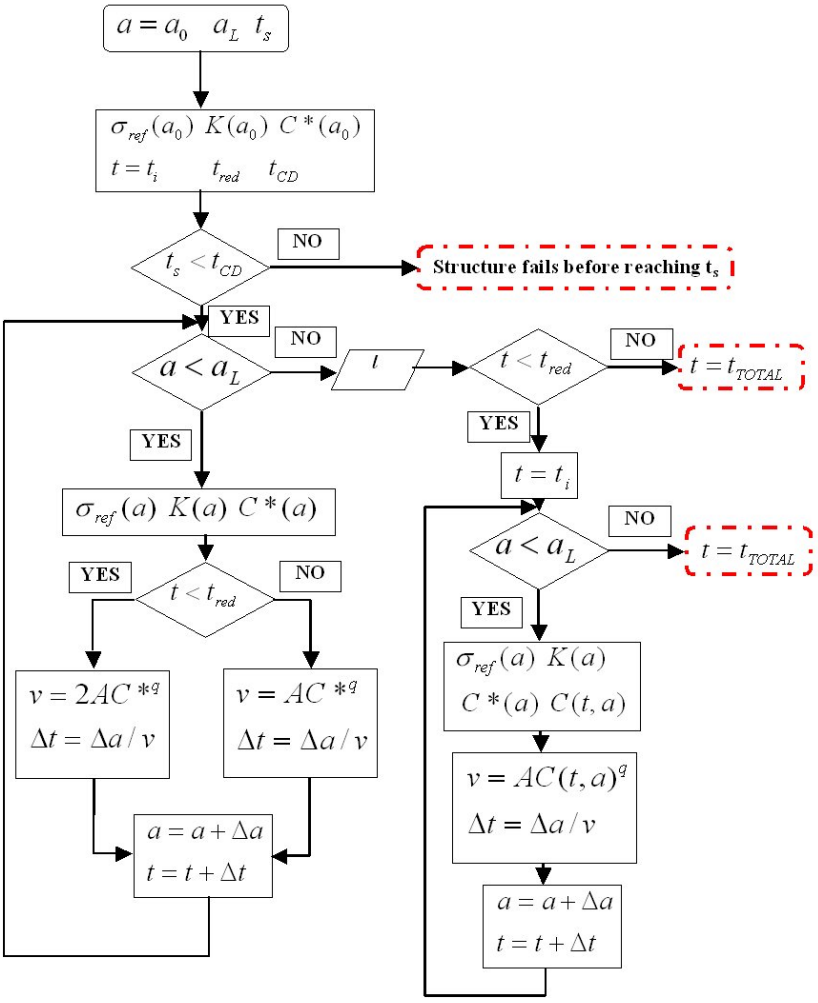

Figure 3.2: Flowchart of the R5 creep crack growth assessment procedure.

prediction is the size of this crack increment which can describe the level of required precision of computation. Therefore some sensitivity analysis was performed. In the R5 and A16 procedure the increment was increased between 0.001-1. mm. The JNC method operates with two kinds of increments. The first one corresponds to increments in the other methods and is used for computation of the lifetime. The second one (ΔA)is used for the computation

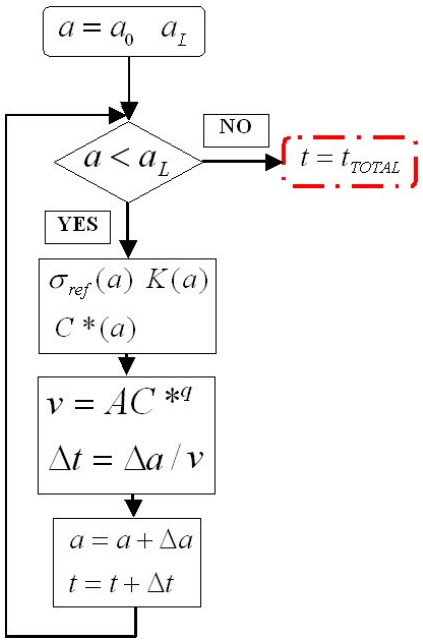

Figure 3.3: Flowchart of the A16 creep crack growth assessment procedure.

of the stress relaxation. This increment must be larger than the increment Δa. The size of the increment ΔA was chosen between 0.01-1 mm. The second increment was then taken in the particular cases from 0.001 to the size of ΔA. The graphical results of the sensitivity analysis are shown in the figure 3.5.

This figure shows very strong dependence of the JNC procedure on the value of ΔA. With increasing value of ΔA increases the total lifetime. This is caused by the fact that the stress relaxation plays more significant role. For the chosen ΔA the change of the Δa does not produce significant differences of the total lifetime. The plot shows also the extreme case of $\Delta A = \Delta a$. In this case the procedure predicts extremely short lifetimes because no stress relaxation is taken into account. The other two methods do not show the significant dependence on the size of Δa. The increase occurs only for large Δa. The differences between the R5 and A16 procedures are not significant and the difference is caused by the factor E/E^* in the definition of C^* in A16 procedure. The prediction of the crack growth

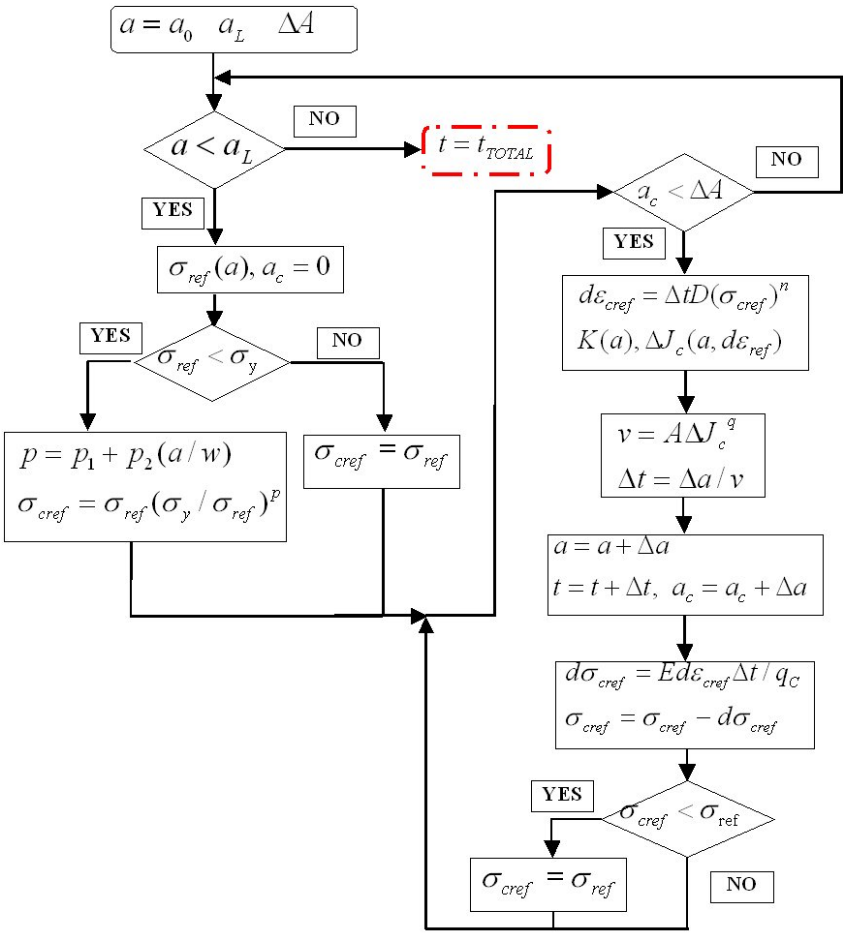

Figure 3.4: Flowchart of the JNC creep crack growth assessment procedure.

during the lifetime is shown in the figure 3.6 for (Δa = 0.01, ΔA = 0.1). JNC method predicts significantly smaller crack growth rate while the curve for R5 and R16 are very close to each other.

The other sensitivity analysis is performed for R5 procedure with respect to the material parameters used in the method. Those parameters are D, n from the Norton's creep law and A, q from the creep crack growth law. The influence of the given parameter change

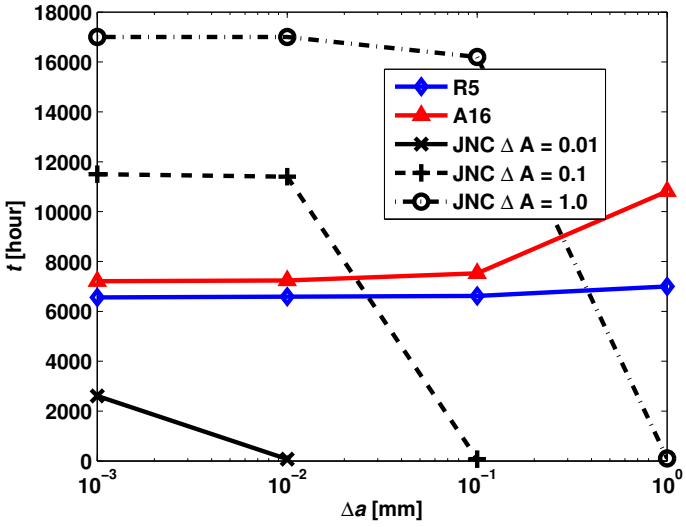

Figure 3.5: Sensitivity of the lifetime prediction with respect to the chosen crack increment Δa for different assessment methods.

to the resulting lifetime prediction is shown in figure 3.7(a-d). This procedure is highly sensitive to the parameters q and n which are the exponents in the formulas. The change in the prediction of lifetime by order of magnitude can be caused by the change of q by 0.1 and n by 1. The sensitivity with respect to the A and D is much smaller. When these parameters increase by the order of magnitude, the lifetime decreases by the order of magnitude. This means that especially exponent parameters must be measured with high precision for obtaining the good quality predictions. Another parameter which is very important is plastic collapse load which is used in computation of σ_{ref}. This reference stress is in the formula for C^* with exponent $n-1$. If the material has this creep exponent high, the reference stress strongly influenced the C^* and lifetime prediction in consequence. Therefore it is necessary to estimate very precisely the collapse loads of the structures made by these materials. This is particularly the case of EUROFER steel where the $n = 17.169$ for 550 $°C$.

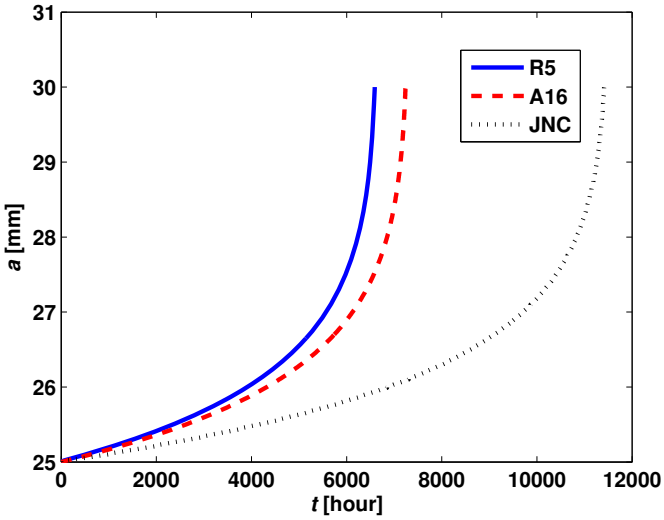

Figure 3.6: Creep crack growth prediction on the chosen crack increments $\Delta a = 0.01$, $\Delta A = 0.1$ for different assessment methods.

3.1 Conclusion

The main methods for defect assessment at high temperature conditions were presented. The method which uses the FAD diagram was only described. The methods which predict directly the creep crack growth during the time were tested and analyzed in the example of creep crack growth in CT specimen. This analysis shows that the A16 and R5 procedure provides similar results of creep crack growth. JNC method strongly depends on the chosen size of the crack increments used in the stress relaxation. Therefore this increment must be estimated from the experimental measurements of stress relaxation for given material and structure geometry. As the most suitable procedure for the creep crack growth estimation looks to be R5 procedure which does not need extra parameters like JNC one and it is suitable to describe the transient state before the creep condition are fully established. Therefore this procedure was chosen for further comparison with finite element simulations of different geometries.

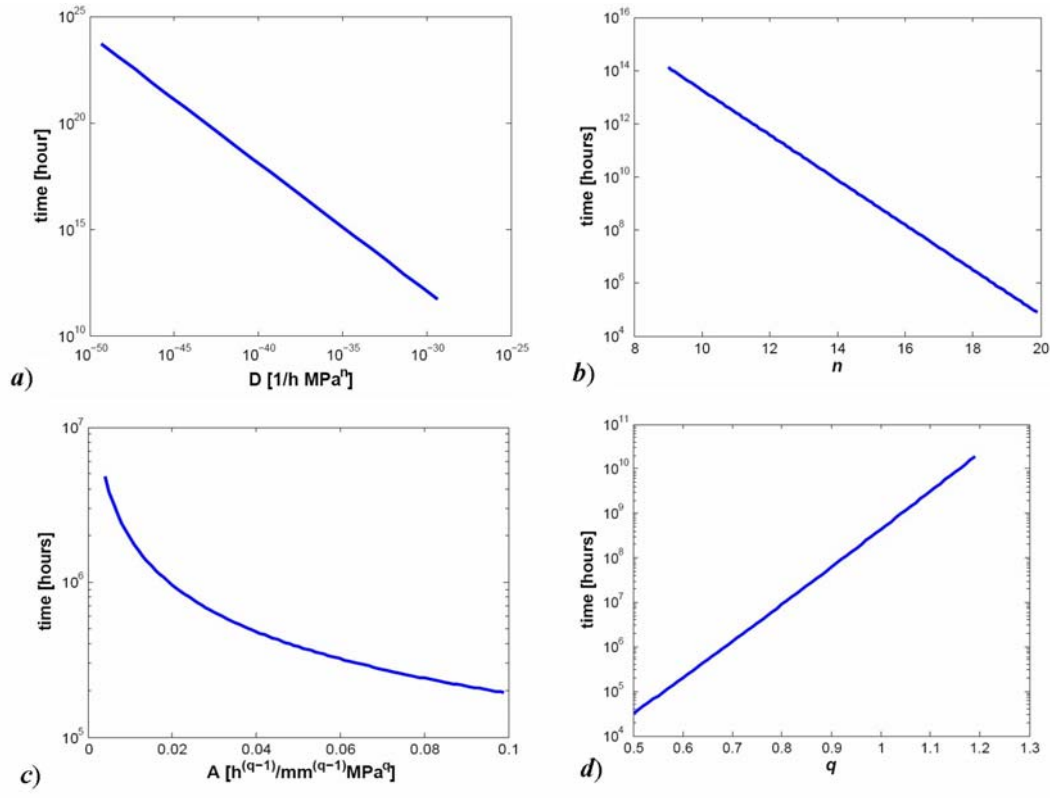

Figure 3.7: Sensitivity of the R5 predicted lifetime on the parameters used in the procedure.

Chapter 4

Verification of the R5 procedure by finite element method for different geometries

The R5 procedure estimations are verified for different geometries using the finite element computations. These chosen geometries are:

- CT specimen
- Cylinder with fully circumferential internal or external crack
- Cylinder with semielliptical circumferential crack.

The crack in these simulations is supposed to be static. Therefore the validation is based on the comparison of the evolution of $C(t)$ parameter and its equilibrium C^* value respectively. This quantity is in R5 given by equation:

$$\frac{C(t)}{C^*} = \frac{(1 + t/t_{red})^{n-1}}{(1 + t/t_{red})^{n-1} - 1} \tag{4.1}$$

where t_{red} is redistribution time when the creep strain reaches the value of initial elastic strain. This time is computed as:

$$t_{red} = \frac{1}{ED\sigma_{ref}^{(n-1)}} \tag{4.2}$$

Finite element simulations are performed by the ABAQUS code. The FE computations of $C(t)$ are based on the evaluation of this parameter in the subsequent contours around crack tip. First contour corresponds to the crack tip and subsequent contours consist of rings of elements around crack tip. The first contour has usually the smallest precision. The value of the $C(t)$ integral depends on the shape of the domain which is embedded by given contour. When the equilibrium value of C^* is reached it becomes to be independent of the domain shape. Therefore in equilibrium conditions the different contours should provide the same values. Because the crack is static, the elements near the crack tip can be theoretically infinitely deformed by creep. Such deformation influences the final value of C^*. This situation cannot occur in the real structure where the creep crack growth occurs and the new stress/strain conditions around the crack tip are established. Therefore the limit of maximal creep strain in the first element ahead of the crack tip is set. This limit is derived from the uniaxial creep (failure) strain ε_f and for the plain strain conditions is equal to $\varepsilon_f/30$. The value of uniaxial creep strain is set as 20% which approximately represents the value for P91 steel which has similar chemical composition as EUROFER steel [17].

The material properties corresponds to EUROFER steel at the temperature 550°C supposed to be the perfectly plastic material. Properties are given in the table 4.1

Material properties of EUROFER steel				
Young's modulus E [GPa]	Poisson's ratio ν	Yield stress σ_y [MPa]	D	n
184	0.3	354	4.566 $\times 10^{-35}$	17.769

Table 4.1: Properties of the EUROFER steel at 550°C

4.1 CT specimen

The first chosen geometry is CT test specimen. This geometry was chosen as starting one for its well established formulas for stress intensity factor and reference stress. This allows to compare the values of $C(t)$ given by formulas and by finite element simulations. The

simulations are performed in 2D because of the symmetry in the thickness direction. The specimen geometry and the finite element mesh are shown in figure 4.1. The specimen dimensions and loading force are shown in table 4.2.

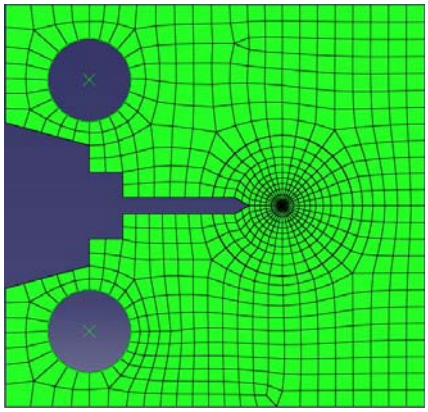

Figure 4.1: The geometry of CT specimen and the chosen finite elements mesh.

width w	initial length a_0	loading force [N]
50	28.82	120

Table 4.2: Dimensions and loading force for CT specimen in finite element simulations.

The equations for the calculation of the stress intensity factor and reference stress are given in the chapter 3 (equations 3.1–3.4.) The comparison of the $C(t)$ estimated by R5 procedure and calculated by finite elements is shown in the figure 4.2. In this case the results show the good correspondence between the theoretical and numerical results. The finite element simulation shows only the slower decay of $C(t)$. This difference is caused by the fact that the R5 formula is derived for general cases therefore its match with particular geometries could not be perfect.

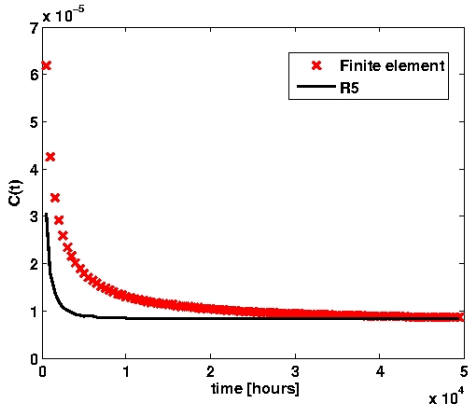

Figure 4.2: Time evolution of $C(t)$ estimated by FE simulation and R5 procedure.

4.2 Cylinder under internal pressure with fully circumferential crack

Because of the symmetry, these simulations are performed as 2D axisymmetric ones. These simulations contains two different cases-internal and external crack. The dimensions and loading are given in the table 4.3.

inner radius r_i [mm]	outer radius r_o [mm]	crack length a [mm]	internal pressure p [MPa]
10	13	1.5	5

Table 4.3: Dimensions and loading of cylinder in finite element simulations.

Images of the overall mesh and the crack tip mesh detail are shown in the figure 4.3.

For the R5 procedure it is necessary to have the formulas for stress intensity factor and reference stress. The solution for stress intensity factor exists only for the case of the tube under tensile loading [18]. But axial stress (σ_{33}) is the most important component for the stress intensity factor evaluation in the case of circumferential crack in the cylinder under internal pressure. Therefore the FE solutions of the cylinder under tensile and internal

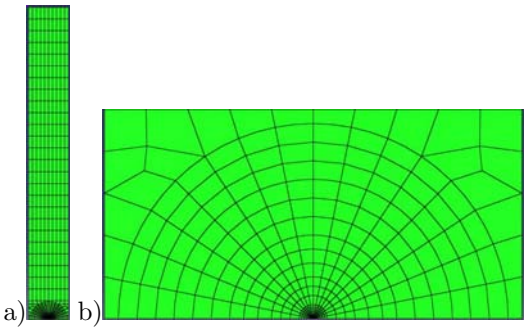

Figure 4.3: Geometry and mesh of the 2D axisymmetric simulation of the cylinder a) whole mesh b) detail of the crack tip mesh.

pressure loading are compared with analytical solution. The results are shown in the figure 4.4.

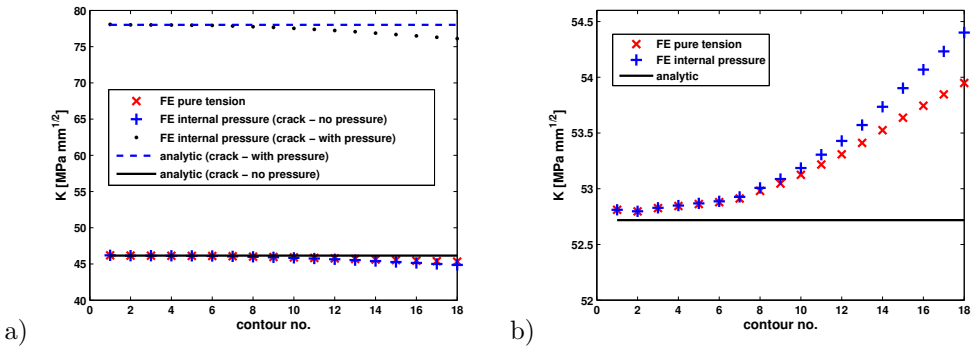

Figure 4.4: Comparison of the stress intensity factors estimated by FE simulations with results provide by handbook formula for a) internal crack, b) external crack.

Figure a) is for internal crack and case b) is for external crack. For the internal crack are included cases with and without pressure at the crack surface. The results show very good correspondence between the analytical and numerical solutions. The differences between the analytical and finite element solution is within the 2.7% for internal crack and 3% for external crack. This means that the formulas for pure tension can be applied for the case of the cylinder under internal pressure. The stress intensity factor can be computed according

the relations:

$$K(a,\beta,\gamma) = F(\beta,\gamma)P\sqrt{\pi a} \quad \beta = a/(r_o - ri) \quad \gamma = r_i/r_o \tag{4.3}$$

$$F(\beta,\gamma) = 1.117 + \Omega_1\beta + \Omega_2\beta^2 + \Omega_3\beta^3 + \Omega_4\beta^{4\gamma+5} + \Omega_5\beta^{24\gamma+6} \tag{4.4}$$

$$\Omega_i(\gamma) = A_{i1} + A_{i2}\sqrt{\gamma} + \frac{A_{i3}}{1.2-\gamma} + \frac{A_{i4}}{(1.05-\gamma)^2} + \frac{A_{i5}}{(1.008-\gamma)^4} \tag{4.5}$$

for internal crack, where coefficients A_{ij} can be found in [18], $P = \sigma_{33}$ for crack without surface pressure and $P = p + \sigma_{33}$ with surface pressure. Stress intensity factor for external crack is given by formula:

$$K(a,\beta,\gamma) = F(\beta,\gamma)P\sqrt{\pi a} \quad \beta = a/(r_o - ri) \quad \gamma = r_i/r_o \tag{4.6}$$

$$F(\beta,\gamma) = 1.121 + \sum_{i=1}^{5} \Omega_i(\gamma)(\beta^2)^{i-1} \tag{4.7}$$

$$\Omega_i(\gamma) = A_{i1} + A_{i2}\sqrt{\gamma} + \frac{A_{i3}}{2.2-\gamma} + \frac{A_{i4}}{(1.05-\gamma)^2} + \frac{A_{i5}}{(1.01-\gamma)^4} \tag{4.8}$$

where $P = \sigma_{33}$. The value of reference stress is obtained according to relations for limit yield pressure derived in [19] which were established on the base of finite element simulations. For the internal crack without pressure at the crack surface, the limited yield pressure can be obtained as:

$$P_L = H\sigma_y \ln\frac{r_o}{r_i} + H\sigma_y min(0,g) \tag{4.9}$$

$$g = f\left[\left(\frac{r_i+a}{ri}\right)^2 \ln\frac{r_o}{r_i+a} - \ln\frac{r_o}{r_i} + \frac{r_i^2 - (r_i+a)^2}{2r_i^2}\right] + \frac{r_o^2 - r_i^2}{2r_i^2} \tag{4.10}$$

where H is the factor depending on the yield criterion: $H = 1$ for Tresca and $H = 2/\sqrt{3}$ for von Mises. Parameter f is the function describing the angle size of the crack in the peripheral direction. For fully circumferential crack is $f = 1$ and for other cases is given as:

$$f = \frac{\theta}{\pi} + \frac{2}{\pi}\arcsin\left(\frac{1}{2}\sin\theta\right) \tag{4.11}$$

where 2θ is the periphery angle occupied by the crack. For the case with surface crack under pressure the limit yield pressure is expressed as:

$$P_L = H\sigma_y \left(f \ln \frac{r_o}{r_i + a} + (1 - f) \ln \frac{r_o}{r_i} \right) + H\sigma_y min(f \frac{a}{r_i + a}, g) \tag{4.12}$$

$$g = \frac{1}{2} \left[\left(\frac{r_o}{r_i + a} \right)^2 - 1 \right] + (1 - f) \left[1 - \left(\frac{r_i}{r_i + a} \right)^2 \right] \tag{4.13}$$

and for the case of the external circumferential crack

$$P_L = H\sigma_y min(\ln \frac{r_o}{r_i}, g) \tag{4.14}$$

$$g = \frac{f[(r_o - a)^2 \ln((r_o - a)/r_i) + 1/2((r_o - a)^2 - r_i^2)] + (1 - f)[r_o^2 \ln(r_o/r_i) + 1/2(r_o^2 - r_I^2)]}{f(r_o - a)^2 + (1 - f)r_o^2} \tag{4.15}$$

These equations gives the plastic collapse load 103.43 MPa for internal crack with pressure and 92.63 MPa for external crack. The FE simulations provide the values of 102.9 MPa for internal crack and 92.1 MPa for external crack. These differences are small within 0.2% but due to the high value of creep law exponent for EUROFER steel, the small changes in plastic collapse load can caused large differences in R5 procedure prediction of $C(t) - C^*$ parameter. These differences in stress intensity factor and plastic collapse load gives according to equation 2.7 the interval of dispersion of $C(t) - C^*$ values within 15% for internal crack with pressure and 17% for external crack. The results of $C(t)$ for the internal crack with pressure at the crack surface are shown in the figure 4.5. Figure a) shows the time evolution of $C(t)$ for the first and the last contour and R5 computation. Case b) then shows comparison of the values for the given time (t = 2.5 $\times 10^8$) in which the creep strain limit was reached. The R5 estimations are computed from the analytical values of K and P_L. The time evolution corresponds quite well for R5 and finite element simulations. Comparison of the R5 estimate and FE results shows maximal difference about 18%. This corresponds to the before estimated interval. The possible differences can be caused by the fact that the solution for plastic collapse load is derived from FE simulations too and has only limited precision. The decrease of values for higher contours in the figure b) can be caused by the

fact that the creep strain limit is reached also in some parts of elements which are further ahead of the crack tip therefore the real crack could propagate earlier.

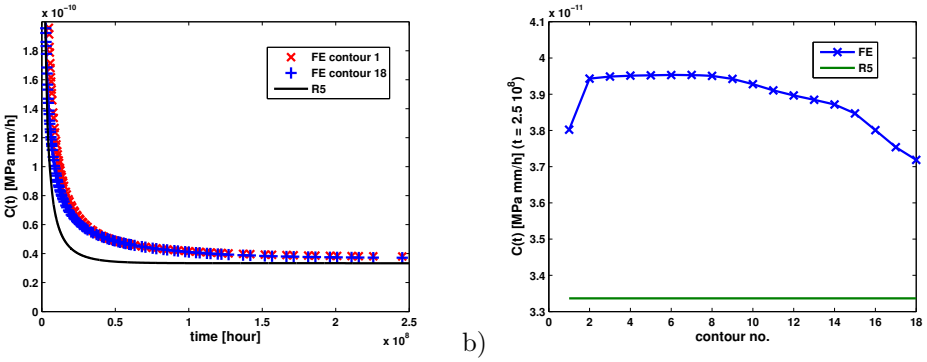

a) b)

Figure 4.5: Comparison of $C(t)$ estimated by FE simulations and R5 for the cylinder subjected to the internal pressure with fully circumferential internal crack with pressure at the crack surface a) time evolution, b) contour values convergence.

The values for the external crack case are shown in the figure 4.6. Figure a) shows that in this case there are big differences in the decay of $C(t)$ values. This may be caused by the higher rate of stress relaxation in the finite element simulations. The comparison of values at the same time is in very good correspondence with difference of order of 7% as it is shown in the figure b) as well as the good convergence of the $C(t)$ value with increasing number of contours.

4.3 Cylinder under internal pressure with semielliptical circumferential crack.

This investigated case is the most complex one and requires 3D simulation. Because of the symmetry only quarter of the cylinder is modeled. The images of the whole mesh and the details of the crack mesh are shown in the figure 4.7. The dimensions and the pressure are given in the table 4.4.

The comparisons are done for the point of the deepest crack which is the most important from the point of view of the crack propagation and structure lifetime. The formula for stress

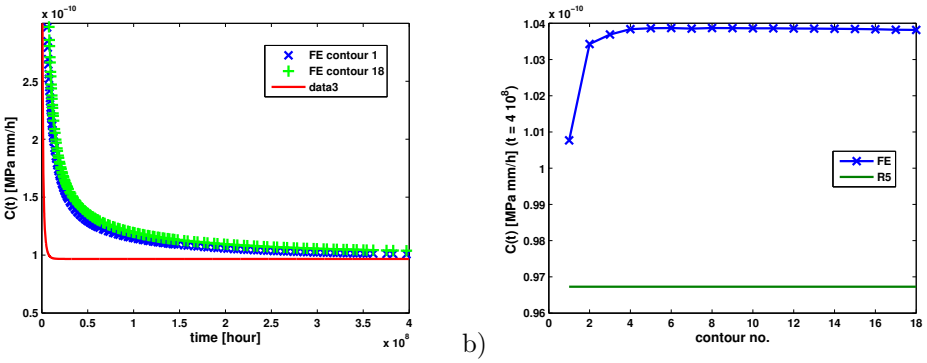

Figure 4.6: Comparison of $C(t)$ estimated by FE simulations and R5 for the cylinder subjected to the internal pressure with fully circumferential external crack a) time evolution, b) contour values convergence.

inner radius r_i [mm]	outer radius r_o [mm]	crack depth a [mm]	crack length $2c$ [mm]	internal pressure p [MPa]
15	18	1.8	7.2	10

Table 4.4: Dimensions and loading of cylinder with semielliptical crack in finite element simulations.

intensity factor is given only for special combinations of crack size and wall thickness and for the tensile loading [18]. The compatibility of this solution with the internal pressure loading is shown in the figure 4.8. The differences between the FE results and values computed according the handbook formula are within 1.5%. These results also show that the formula for pure tension can be used also for the internal pressure loading case. For pressure free crack can be used without changes and for crack under pressure is loading equal to the sum of the axial stress and applied pressure ($\sigma_{33} + p$).

The formula for limit yield pressure for cylinder with semielliptic crack does not exist. Therefore the plastic collapse loads were taken from FE simulations and also the formulas for rectangular cracks were taken as an approximation [19]. The size of the rectangular crack is chosen in that way that the surface area is equal to the semielliptic crack and the crack depth is equal to the biggest depth of the semielliptic crack. FE simulations provide the

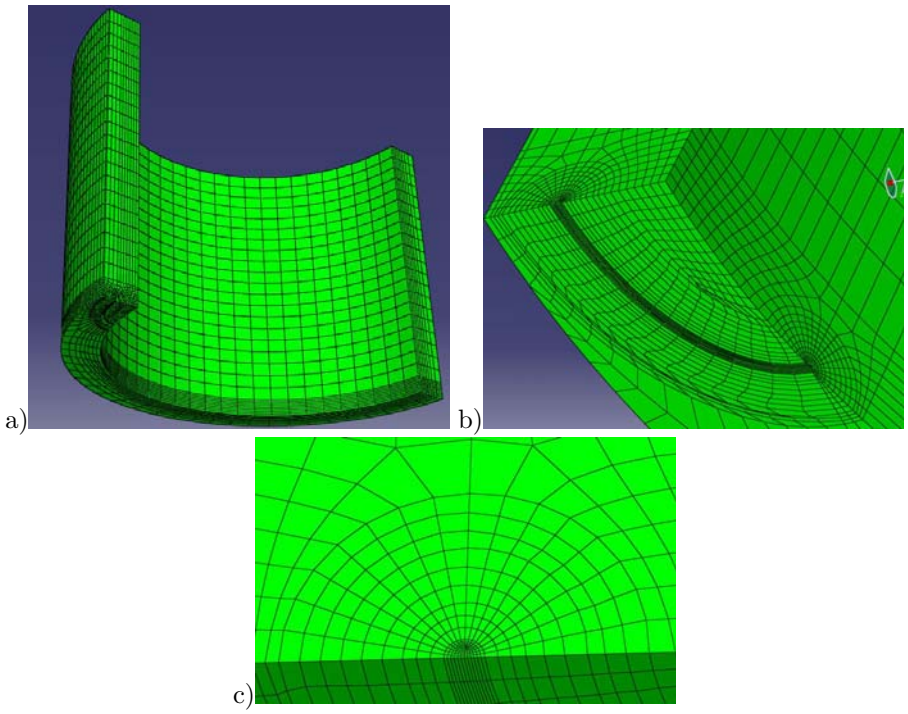

Figure 4.7: Geometry and mesh of the 3D simulation of the cylinder a) whole mesh b) detail of the crack area mesh c) detail of the crack tip mesh at the midpoint of the crack.

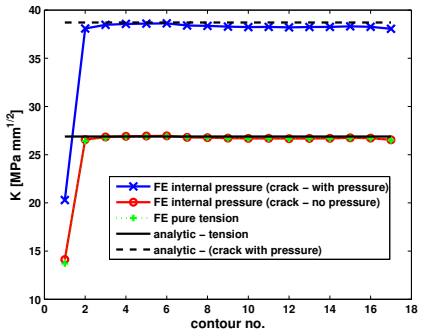

Figure 4.8: Comparison of stress intensity factors for different loading cases estimated by FE simulations and relations from handbook.

collapse load of 74.56 MPa for crack without pressure and 74.58 MPa for pressurized crack. The rectangular crack approximation then gives: 74.53 MPa for crack without pressure and 74.23 MPa for crack with pressure. The differences are smaller than 0.5%. Even these small differences can cause the dispersion of C^* values about 14% for crack with pressure and 4% for crack without pressure.

The results for the crack without pressure are shown in the figure 4.9. Figure a) shows the different shape of the curves for particular contours. This is due to the domain shape dependency during the initial phase. In the equilibrium state all curves converge towards one value which is very close to the R5 one (difference of order of 3.7%). Figure b) demonstrates the good convergence of the values except of the first contour, but this one is usually less precise.

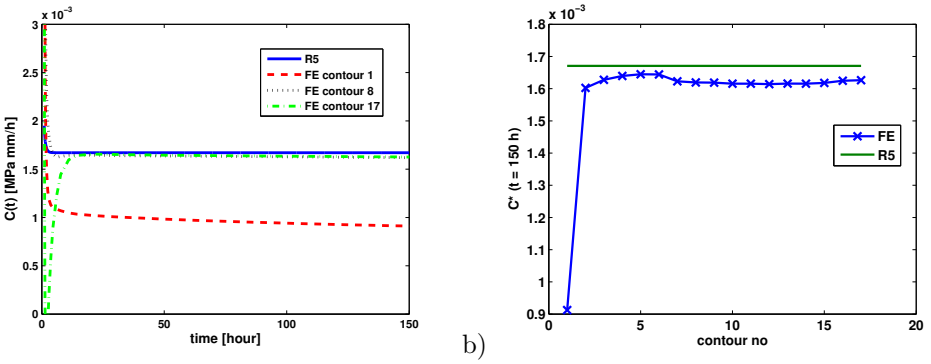

a) b)

Figure 4.9: Comparison of $C(t)$ estimated by FE simulations and R5 for the cylinder subjected to the internal pressure with semielliptic circumferential internal crack (crack surface without pressure) a) time evolution, b) contour values convergence.

Similar results are obtained for the crack with applied pressure. These results are shown in the figure 4.10. There is again domain dependence for $C(t)$ values at the beginning. The equilibrium values are with good agreement with the R5 prediction. Differences are larger than in the previous case but still in the expected error range of 14%. These larger differences are caused by the higher stresses at the crack tip region which results in the higher element deformation which may cause differences in the resulting $C(t)$ values. The

convergence of the solution is good for different contours except the first one as shown in the figure b).

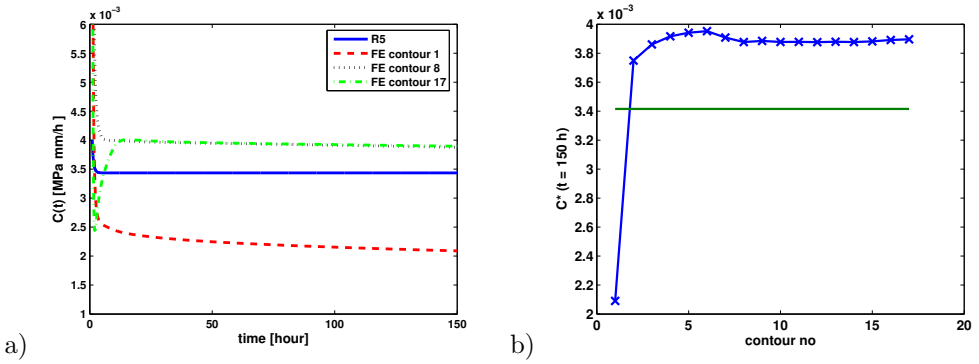

Figure 4.10: Comparison of $C(t)$ estimated by FE simulations and R5 for the cylinder subjected to the internal pressure with semielliptic circumferential internal crack (crack surface with pressure) a) time evolution, b) contour values convergence.

4.4 TBM like shape structure

The last example for verification is 2D simulations which are performed with a structure representing a section of the test blanket module (TBM). This structure is shown in figure 4.11 a) with its dimensions. This investigated structure corresponds to the shape which shall be used in mock–up experiment which should demonstrate the properties and abilities of the TBM design. This module is subjected to a thermomechanical loading which consists of the three main parts (see fig. 4.11b)):

- Internal pressure in the cooling channels.
- Temperature at the cooling channels surfaces.
- Heat flux at the left surface of the module

Investigation of the stress/strain distribution in the structure shows that the highest stress concentration occurs in between the cooling channels at the vertical axis of the struc-

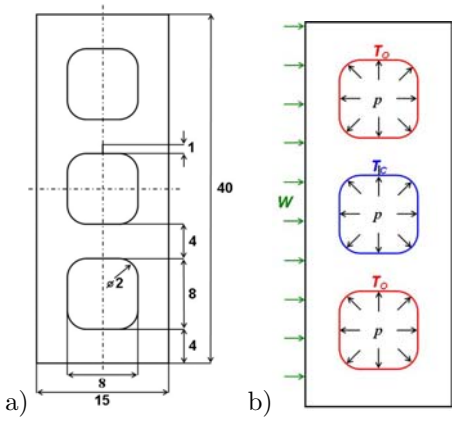

Figure 4.11: Geometry and dimensions of TBM structure a) and thermomechanical loading conditions b)

ture. Therefore the 1 mm long crack is placed in the middle of the upper surface of the central cooling channel (see fig.4.11a)).

According to these loading conditions 8 different cases are investigate (see 4.5):

case no.	$T_o[°C]$	$T_c[°C]$	$W[kW/m^2]$	pressure p [MPa]	p at crack	mesh type
1	350	300	300	10	no	full
2	550	550	300	10	no	full
3	350	300	0	10	no	full
4	550	550	0	10	no	full
5	350	300	0	10	no	half
6	550	550	0	10	no	half
7	350	300	0	10	yes	half
8	550	550	0	10	yes	half

Table 4.5: Different cases of loading in simulations: T_o–temperature of outer channels, T_c–temperature of central channel, W–surface heat flux, p–pressure in the channels.

The first temperature distribution ($T_o = 350°C$, $T_c = 300°C$) is chosen according to the results of [20] where this case was found as the worst with respect to the damage evolution. The second case ($T_o = T_c = 550°C$) is chosen as a representative of the high temperature state. The pressure p is chosen higher than the one which will be supposed in

the real application (about 8 MPa). Two kinds of simulations are performed with respect to the applied pressure. One supposed the crack flaws without pressure and the other with pressurized crack flaws. The first case is modeled with the full structure mesh, the second can be modeled only with half of the structure. Both cases of used mesh are shown in figure 4.12.

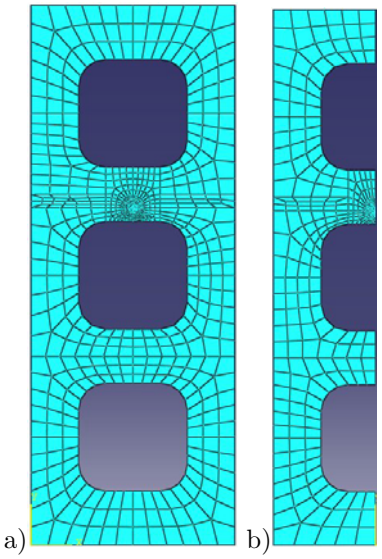

Figure 4.12: Meshes for TBM structure simulation a) full structure b) half structure.

Due to the asymmetry of the heat flux application, this boundary condition cannot be applied in the half mesh simulations. Therefore it is necessary check the temperature distribution around the crack tip for the case with and without applied heat flux (case 1 vs. case 3, case 2 vs. case 4) as well as the differences between the full mesh and half mesh simulations (case 3 vs. case 5, case 4 vs. case 6).

Because the temperature distribution considered here, the material parameters must be taken as temperature dependent. The data for Young's modulus and yield stress are taken from [21]. Heat conductivity is from [22]. The creep parameters are in both cases taken for temperature 550 $°C$.

Comparison of the temperature fields for the case with and without heat flux shows no differences around the crack tip so within these conditions are the two cases equivalent. In this case the stress intensity factor and plastic collapse load cannot be computed from some formulas, therefore all values are obtained by the finite element simulations. The differences of the stress intensity factor values with respect to the contours around the crack tip does not exceed 2% and differences between compared cases (1-3, 2-4, 3-5, 4-6) are around 0.5%. The plastic collapse load was defined as the pressure value in the cooling channel when the wall between channels collapses. This collapse occurs when there is continuous area with plastic strain higher than 0.2% connecting two cooling channels. This kind of collapse occurs first in the wall which contains crack. Identification of the right collapse load value is very important due to the sensitivity of the R5 procedure on its value. In these cases the interval of values were estimated and for further computations the mean values from these intervals were taken. But the scatter of the values in interval is about 6% which may result in large discrepancies in R5 predictions. The values of plastic collapse load for different cases are shown in the table 4.6

case no.	$P_L[MPa]$
1	163.13
2	124
3	163.13
4	123.75
5	163.75
6	123.8
7	147.75
8	111.25

Table 4.6: Plastic collapse load for different boundary conditions cases.

The results of $C(t)$ for different cases are shown in figures 4.13–4.20 a),b). Plots a) show the time evolution of $C(t)$ parameter and comparison of R5 predictions with FE results for given contours around crack tip. Plots signed as b) then show the comparison of R5 prediction with FE results at the time when the creep strain limit is reached.

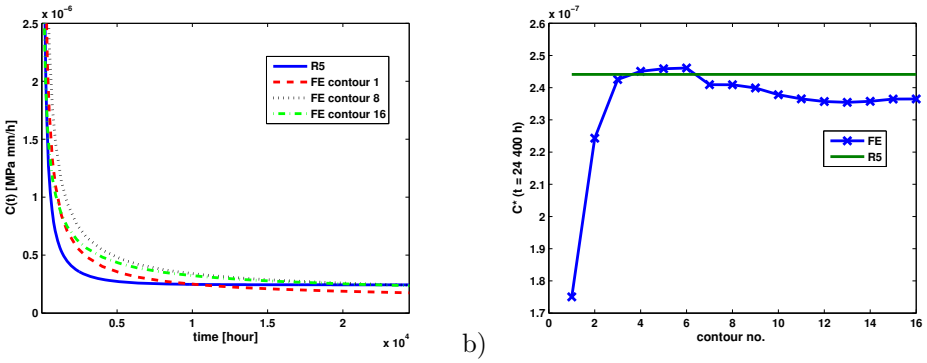

a) b)

Figure 4.13: Comparison of $C(t)$ estimated by FE simulations and R5 for the TBM mock–up for case 1 of a) time evolution, b) contour values convergence.

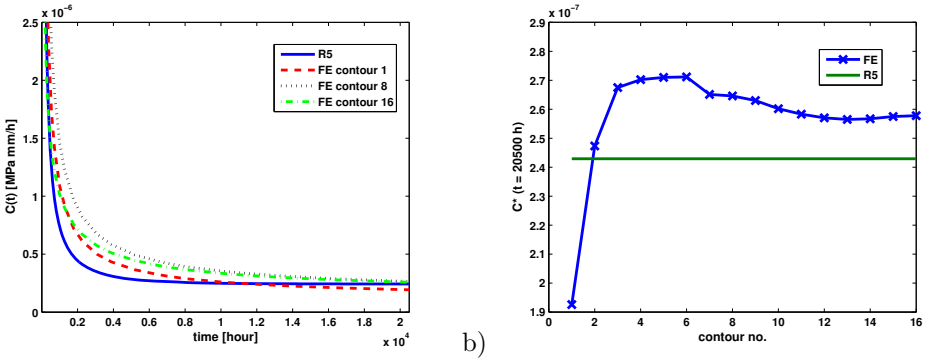

a) b)

Figure 4.14: Comparison of $C(t)$ estimated by FE simulations and R5 for the TBM mock–up for case 2 of a) time evolution, b) contour values convergence.

The time evolution shows good correspondence between R5 and FE predictions. The R5 has steeper decrease and reach the equilibrium values in shorter time. This could be related to the general manner of the R5 formulas which are not focused on particular geometries. The FE results also show the permanent decrease but this is caused by the static crack and deformation of elements which is not physically reasonable after certain limit. The comparisons of the FE results with R5 at the creep strain limit time show also the good accordance. The differences are within 10% for the case with press free crack and

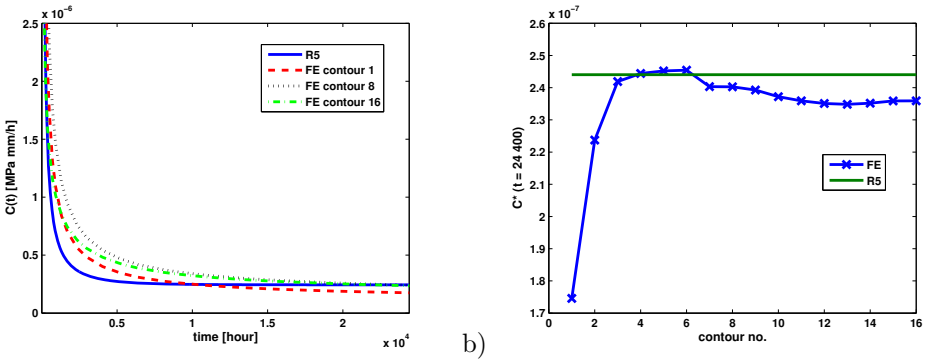

a) b)

Figure 4.15: Comparison of $C(t)$ estimated by FE simulations and R5 for the TBM mock–up for case 3 of a) time evolution, b) contour values convergence.

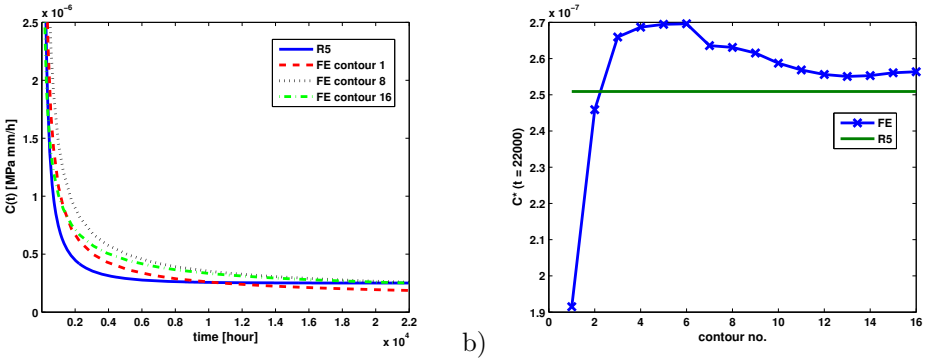

a) b)

Figure 4.16: Comparison of $C(t)$ estimated by FE simulations and R5 for the TBM mock–up for case 4 of a) time evolution, b) contour values convergence.

within 18% for pressurized crack cases. The compared cases (1-3, 2-4, 3-5, 4-6) have very small differences in $C(t)$ values which means that the applied heat flux does not strongly influence the stress distribution at the crack tip. These results state also that simulation of half structure provides the same results as full structure ones. The difference is notable in the prolongation of the time when the creep strain limit is reached for half structure simulations. The increase of temperature causes the decrease of the reaching of the limit time about 19%. The situation is dramatically changed when the pressure is applied at the

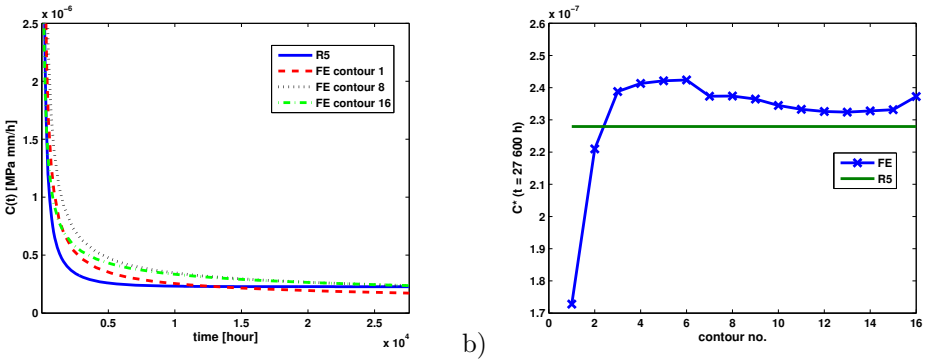

a) b)

Figure 4.17: Comparison of $C(t)$ estimated by FE simulations and R5 for the TBM mock–up for case 5 of a) time evolution, b) contour values convergence.

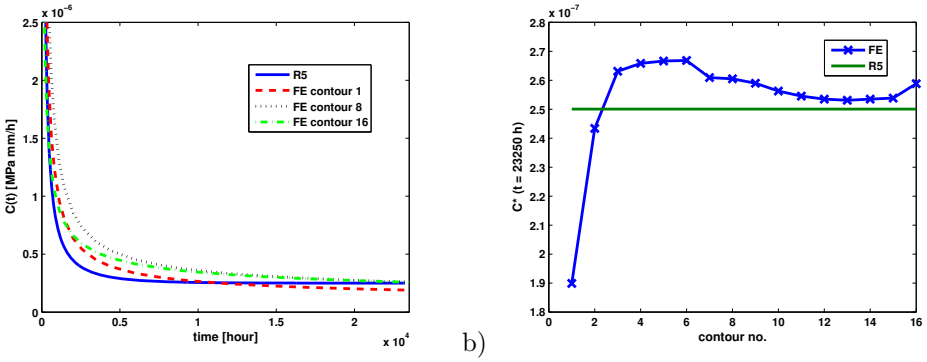

a) b)

Figure 4.18: Comparison of $C(t)$ estimated by FE simulations and R5 for the TBM mock–up for case 6 of a) time evolution, b) contour values convergence.

crack flaws. Values of $C(t)$ increase by the order of magnitude and the time for reaching the creep strain limit decreases towards 1500 hours for case 7 and 1100 hours for case 8 respectively. These results can predict the durability of this component under complex loading and this structure is able to sustain these conditions for given crack length for over 1000 hours before the crack starts to propagate.

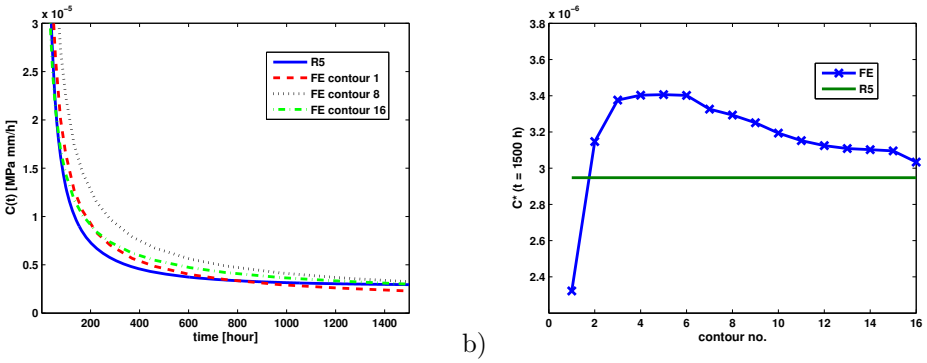

a) b)

Figure 4.19: Comparison of $C(t)$ estimated by FE simulations and R5 for the TBM mock–up for case 7 of a) time evolution, b) contour values convergence.

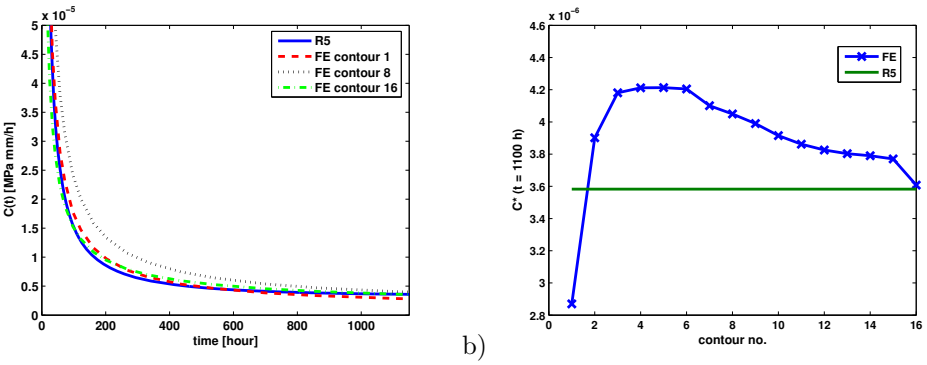

a) b)

Figure 4.20: Comparison of $C(t)$ estimated by FE simulations and R5 for the TBM mock–up for case 8 of a) time evolution, b) contour values convergence.

4.5 Conclusion

The results of this section show the comparison of the estimates provide by finite element simulations and R5 procedure for different geometries. These estimates are in the good accordance and show the suitability of the R5 procedure to describe the creep conditions at the crack tip. This comparison also shows some limitations and possible ways to improvement this procedure. The decay of $C(t)$ value is steeper in R5 estimation. Therefore the formula for its calculation could be improved. This could be done by the description of

the stress redistribution during the transient creep period which will influence the reference stress and value of redistribution time. The simulations with the TBM structure also show the durability of this component which can be roughly estimated as the order of tens of thousands hours.

Chapter 5

R5 application handbook

In this chapter is described the handbook for the application of R5 procedure in praxis. For the given structure must be given:

- Initial crack length (a_0)
- Stress distribution or loading conditions
- Plastic collapse load for given loading conditions measured experimentally or estimated from analytical formulas or FE element simulations.

Estimation of times used in R5: Time for creep damage to propagate through structure and lead to failure (t_{CD}):

$$t_{CD} = t_r[\sigma_{ref}(a_0)] \tag{5.1}$$

Time t_r is obtained from the stress/time to rupture data so the creep rupture experiment must be performed for this estimation.

Redistribution time (t_{red}): This time covers the period during which the initial elastic strain is relaxed by creep. This is expressed by the equation:

$$\varepsilon_c[\sigma_{ref}(a_0, t_{red})] = \sigma_{ref}(a_0)/E \tag{5.2}$$

The reference stress and its possible time evolution (depends on the boundary conditions) must be evaluate to get the redistribution time interval. (Example: For the constant

reference stress and secondary creep described by Norton's law ($\dot{\varepsilon} = D\sigma^n$), the redistribution time is given by equation: $t_{red} = 1/ED(\sigma_{ref}(a_0))^{n-1}$.)

Initiation time (t_i): There must be performed creep crack growth experiments for estimation of this time. Initiation is defined as a period when the crack extents by 0.2 mm. There are three possibilities to estimate the initiation time.

- Initiation time can be correlated with C^* parameter by equation:

$$t_i C^{*q} = B \tag{5.3}$$

  Where B is constant. Formulas for C^* are available for basic types of test specimens. Obtaining of this relation is shown in figure 2.2.

- Initiation time can be estimated with measurement of critical crack opening displacement δ_i according the relation:

$$D\sigma_{ref}(a_0)^n t_i = \left(\frac{\delta_i \sigma_{ref}(a_0)^2}{K^2}\right)]^{n/(n+1)} - \sigma_{ref}(a_0)/E \tag{5.4}$$

  Where K is the stress intensity factor.

- Initiation time can be set $t_i = 0$ for conservative estimates.

Propagation time (t_g): This time is estimated according to the creep crack growth law so the necessary parameters are A and q obtained from creep crack growth experiments and its representation in the dependence of creep crack growth rate ($\dot{a}$) with respect to the C^* parameter. For given crack increment (Δa) the propagation time can be estimated:

$$\Delta a = \int_0^{t_g} AC^{*q} dt \tag{5.5}$$

The lifetime estimation then can be computed according to the flow chart shown in figure 3.2.

Chapter 6

Conclusions

The crack assessment procedures for high temperature application are presented and tested in this report. The results can be summarized in the following points:

- The most suitable creep crack growth procedure was found to be R5 which is able to describe the creep crack growth. This method is also able to predict the crack growth during the period before the redistribution of stresses and establishing of equilibrium conditions.
- The R5 procedure is very sensitive to the values of creep crack growth parameters q and n which can strongly influenced the resulting lifetime prediction. Therefore it is necessary to get these parameters as precise as possible.
- For high values of n (EUROFER steel case) the resulting reference stress can strongly influence the lifetime prediction. Therefore it is necessary correctly analyzed loading conditions as well as the plastic collapse load for investigated structure.
- Verification of the R5 procedure by FE based on the comparing of evolution of parameter $C(t)$ shows very good agreement for some basic geometries including: CT specimen, cylinder subjected to internal pressure with fully circumferential internal and external crack, cylinder subjected to internal pressure with semielliptical circumferential crack.

- The R5 procedure is suitable for the prediction of the creep crack growth for the structure which can simulate the TBM component of the ITER as show the comparisons with FE results.
- Very rough estimate of the TBM component durability can be given by performed simulations. The durability could be in the order of tens of thousands of hours.
- The handbook for R5 application was created with description of the necessary data and experiments which must be performed to obtain parameters for lifetime prediction.

Chapter 7

Prospects

- The comparison of R5 with FE element simulations for EUROFER steel parameters including hardening behavior.
- The defect assessment procedures can be implemented into the code and provided as post processing software package.
- Performing the lifetime experiment with mock–up TBM geometry to verify the R5 procedure by experimental results.
- The possible improvements in the assessment procedures can be investigated with respect to the simulations results included for example residual stresses.

Chapter 8

Acknowledgment

This work, supported by the European Communities under contract of Association between EUROATOM and Forschungszentrum Karlsruhe, was carried out within the framework of the European Fusion Development Agreement. The views and opinions expressed herein do not necessarily reflect those of the European Commission.

Chapter 9

IP reporting

All the works provided under the present task were according to the current state–of–the art. No foreground IPR has been produced under this task. All information from involved external companies and sub–contractors is open and available, and no confidentiality or license agreement was signed. No invention or software development has to be declared.

Bibliography

[1] C.S. Wiesner, S.J. Maddox, W. Xu, G.A. Webster, F.M. Burdekin, R.M. Andrews, and J.D. Harrison. Engineering critical analyses to BS 7910 – the UK guide on methods for assessing the acceptability of flaws in metallic structures. *International Journal of Pressure Vessels and Piping*, 77:883–893, 2000. 1, 2.5

[2] R5, assessment procedure for the high temperature response of structures, procedure R5, issue 2 gloucester. *UK:Nuclear Electric Ltd*, 1997. 2.1

[3] D.W. Dean, R. A. Ainsworth, and S.E. Booth. Development and use of the R5 procedures for the assessment of defects in high temperature plant. *International Journal of Pressure Vessels and Piping*, 78:963–976, 2001. 2.1

[4] P.J. Budden. Validation of the high–temperature structural integrity procedure R5 by component testing. *International Journal of Pressure Vessels and Piping*, 80:517–526, 2003. 2.1

[5] R. A. Ainsworth and D.G. Hooton. R6 and R5 procedures: The way forward. *International Journal of Pressure Vessels and Piping*, 85:175–182, 2008. 2.1, 2.4

[6] B. Drubay, S. Marie, S. Chapuliot, M.H. Lacire, B. Michel, and H. Deschanels. A16: guide for defect assessment at elevated temperature. *International Journal of Pressure Vessels and Piping*, 80:499 – 516, 2003. 2.2, 2.3

[7] T. Wakai, B. Poussard, and B. Drubay. A comparsion between japanese and french A16 defect assessment procedures for fatigue crack growth. *Nuclear Engineering and Design*, 212:125–132, 2002. 2.2, 2.3

BIBLIOGRAPHY

[8] T. Wakai, B. Poussard, and B. Drubay. A comparsion between japanese and french A16 defect assessment procedures for creep–fatigue crack growth. *Nuclear Engineering and Design*, 224:245–252, 2003. 2.2, 2.3

[9] R6, assessment of the integrity of structures containing defects, procedure R6, revision 3 gloucester. *UK:Nuclear Electric Ltd*, 1997. 2.4

[10] R. A. Ainsworth. Failure assessment diagrams for use in R6 assessment for austenitic components. *International Journal of Pressure Vessels and Piping*, 65:303–309, 1995. 2.4

[11] R. Wilson. A comparison of the simplified probabilistic method in R6 with the partial safety factor approach. *Engineering Failure Analysis*, 14:489–500, 2007. 2.4, 2.5

[12] R. A. Ainsworth, D.G. Hooton, and D. Green. Failure assessment diagrams for high temperature defect assessments. *Engineering fracture mechanics*, 62:95–109, 1999. 2.4, 2.4

[13] BS 7910:1999 (incorporating amendment no.1): Guide on methods for assessing the acceptability of flaws in metallic structures. *British Standards Institution BSI. London*, 2000. 2.5

[14] A. Kotousov and J.W.H. Price. Elastic analysis of semi–eliptical axial crack in cylinders under thermal shock using the BS 7910 framework. *International Journal of Pressure Vessels and Piping*, 76:831–837, 1999. 2.5

[15] A. Muhammed. Background to the derivation of partial safety factors for BS 7910 and API 579. *Engineering Failure Analysis*, 14:481 – 488, 2007. 2.5

[16] D.W. Dean and D. N. Gladwin. Creep crack growth behaviour of type 316H steels and proposed modifications to standard testing and analysis method. *International Journal of Pressure Vessels and Piping*, 84:378–395, 2007. 3, 3

[17] M. Tan, N. J. C. Celard, K. M. Nikbin, and G. A. Webster. Comparison of creep crack initiation and growth in four steels tested in HIDA. *International Journal of Pressure Vessels and Piping*, 78:737–747, 2001. 4

[18] Y. Murakami. Stress intensity factors handbook (third edition). *The Society of Materials Science, Japan*, 4, 2001. 4.2, 4.2, 4.3

[19] M. Staat and D. K. Vu. Limit loads of circumferentially flawed pipe and cylindrical vessels under internal pressure. *International Journal of Pressure Vessels and Piping*, 83:188–196, 2006. 4.2, 4.3

[20] R. Sunyk and J. Aktaa. Evaluation of ITER design criteria applied to RAFM steels. *Research report FZKA 7241 Forschungszentrum Karlsruhe*, 2006. 4.4

[21] Appendix a – material design limit data: A3.S18E EUROFER steel. *Research report DMN/Dir: NT 2004–D0, CEA,DEN–SAC*, 2004. 4.4

[22] N. Boukos and K. Mergia. Thermal, electrical and ferro–magnetic properties of standard eurofer plate. *Research report, National Centre for Scientific Research "Demokritos"*, www.hellasfusion.gr/Annexes/2002/Annex19.pdf, 2004. 4.4